Time- and cell-resolved dynamics of redox-sensitive Nrf2, HIF and NF-κB activities in 3D spheroids enriched for cancer stem cells

Anna P. Kipp[a,*], Stefanie Deubel[b], Elias S.J. Arnér[c], Katarina Johansson[c,*]

[a] Institute of Nutrition, Department of Molecular Nutrition Physiology, Friedrich-Schiller-Universität Jena, Dornburgerstr. 24, 07743 Jena, Germany
[b] Department of Molecular Toxicology, German Institute of Human Nutrition, Potsdam-Rehbrücke, Arthur-Scheunert-Allee 114-116, 14558 Nuthetal, Germany
[c] Division of Biochemistry, Department of Medical Biochemistry and Biophysics, Karolinska Institutet, SE-171 77 Stockholm, Sweden

ARTICLE INFO

ABSTRACT

Cancer cells have an altered redox status, with changes in intracellular signaling pathways. The knowledge of how such processes are regulated in 3D spheroids, being well-established tumor models, is limited. To approach this question we stably transfected HCT116 cells with a pTRAF reporter that enabled time- and cell-resolved activity monitoring of three redox-regulated transcription factors Nrf2, HIF and NF-κB in spheroids enriched for cancer stem cells. At the first day of spheroid formation, these transcription factors were activated and thereafter became repressed. After about a week, both HIF and Nrf2 were reactivated within the spheroid cores. Further amplifying HIF activation in spheroids by treatment with DMOG resulted in a dominant quiescent stem-cell-like phenotype, with high resistance to stress-inducing treatments. Auranofin, triggering oxidative stress and Nrf2 activation, had opposite effects with increased differentiation and proliferation. These novel high-resolution insights into spatiotemporal activation patterns demonstrate a striking coordination of redox regulated transcription factors within spheroids not occurring in conventional cell culture models.

1. Introduction

Malignant tumors consist of a heterogenic mixture of cancer cells, and only a subset of undifferentiated tumor cells have clonogenic and tumor-initiating potential [1]. These cells are commonly termed 'cancer stem cells' (CSCs) as they share many properties with normal adult and embryonic stem cells [2]. CSCs have unlimited self-renewal capacity, can differentiate asymmetrically, and are believed to drive the heterogeneous cell populations constituting a tumor. They are either slowly proliferating or fully quiescent, and are typically resistant to chemotherapy. Factors and conditions that either control maintenance of undifferentiated clonogenic CSCs or their differentiation into more mature cancer cells are incompletely defined, but redox modulation is likely to be important. Several observations have shown that cancer cells in general have higher endogenous levels of oxidative stress than normal healthy cells [3,4] and thus up-regulate their expression of antioxidant enzymes in order to achieve redox homeostasis and cell survival [5]. How the redox state of CSCs compares to more differ-entiated cells from the same original cancer cell clone is not known. Redox signaling pathways that are activated in response to growth factor stimulation are typically coupled to synthesis of H_2O_2 by NADPH oxidases, but also other sources of H_2O_2 might play a role together with peroxynitrite and lipid hydroperoxides. Many transcription factors are redox regulated, including NF-κB, HIF, Nrf2, Oct-4, β-catenin, Notch, and c-Myc. All of them are known to be important mediators of development and cellular differentiation, but also of cancer promotion [6–8].

NF-κB is involved in cellular responses to inflammation [6]. Under basal conditions, NF-κB is kept inactive in the cytosol by binding to IκB, the inhibitor of NF-κB. Upon activation, a phosphorylation cascade results in the degradation of IκB and nuclear translocation of NF-κB. In relation to colorectal cancer, elevated NF-κB signaling enhances Wnt activation and can support tumor growth [9,10]. Under conditions of constitutively activated Wnt signaling, Rac1-driven H_2O_2 production is also required for NF-κB activation and initiation of colon tumorigenesis [11].

The HIF1 transcription factor consists of two subunits, HIF1β and HIF1α [12]. During normoxia, HIF1α is hydroxylated by prolyl hydroxylase domain proteins (PHD), allowing the recognition and ubiquitination of HIF1α by the Von Hippel-Lindau protein followed by proteasomal degradation. Upon hypoxia (O_2 below 3%), PHDs are inactivated by a shift from Fe^{3+} to Fe^{2+} in their active center. HIF1α becomes stabilized and translocates to the nucleus, where it together with HIF1β induces HIF target genes involved in e.g. the adaptation to hypoxia, angiogenesis, glucose transport, survival and invasion. HIF1α is activated in many different types of cancers, mainly caused by the hypoxic core that develops when tumors grow bigger. For colorectal cancer, it has been shown that hypoxia promotes an aggressive CSC phenotype resulting in invasion and accelerated metastatic outgrowth [13].

During cell homeostasis, Nrf2 is bound to Keap1 and constantly degraded. Upon oxidative or electrophilic stress, Keap1 is modified, whereupon Nrf2 translocates to the nucleus to activate an array of antioxidant and detoxification enzymes, including important proteins of the glutathione (GSH) and thioredoxin systems [6,14,15]. Thus, Nrf2 provides host defense systems that can protect from cancer initiation through more efficient elimination of harmful substances. However, Nrf2 activation in cancer cells can accelerate malignant cell growth [16] and Nrf2 is typically activated in many tumors [17,18]. In Drosophila intestinal stem cells, constitutive Nrf2 activation sustained quiescence by lowering the cellular redox status via up-regulation of genes such as glutamate-cysteine ligase [19].

In the present study, we set out to analyze the activation patterns of Nrf2, HIF and NF-κB in relation to development of spheroids established from individual clones of human HCT116 colon cancer cells. HCT116 cells are known to have a high fraction of CSCs and a low ability to differentiate [20,21]. During the last years, 3D culture models have been increasingly used to study tumor properties and CSC functions, as such cultures are believed to mimic tumor traits better than classical adherent 2D cell cultures. For example, spheroids mirror oxygen and nutrient gradients typical for tumors, such as lower oxygen tension and nutrient supply, but higher lactate concentrations in their cores [22]. Here, HCT116 spheroids were developed under low-attachment culture conditions and with FBS-free medium, which promotes formation of CSCs [23]. To enable studies of the activation of Nrf2, HIF and NF-κB in this system, we stably transfected HCT116 cells with the pTRAF vector (plasmid for transcription factor reporter activation based on fluorescence), which allows for concomitant determination of Nrf2, HIF and NF-κB activation patterns at single-cell resolution by fluorescence detection [24]. In 2D cultures this methodology has revealed a high degree of stochastic variation in these transcription factor activities between individual cells, while here we asked if or how the activation patterns are differently coordinated during development of HCT116 spheroids.

2. Materials and methods

2.1. 2D and 3D cell culture

The human colorectal carcinoma cell line HCT116 was purchased from ATCC (CCL-247) and cultured as described [24]. The 3D spheroids were grown in serum free advanced DMEM/F12 medium (Life Technologies) supplemented as described [23]. To generate 3D cultures, adherently growing cells, derived from a single original clone, were resuspended in stem cell medium at a density of 4000 cells per 100 μl and pipetted into each well of a transparent Nunclon SpheraTM ultra-low surface round bottom 96-well plate (Thermo Fisher; 174925). Whole plates were centrifuged for 5 min at 1200 rpm. One spheroid per well developed within three days, which was monitored daily for up to 14 days.

2.2. qPCR and western blotting

Standard protocols were used to isolate RNA and perform quantitative real-time PCR (Fig. S1A for primers), SDS page, and Western blotting. Further details are described in the supplementary (see primers Fig. S1B experimental setup).

2.3. Stable transfection and pTRAF activity

HCT116 cells were stably transfected with the vector pTRAF[Nrf2/HIF/NFkB], a pGL4.32 vector containing response elements for the transcription factors Nrf2, HIF, and NF-κB in front of sequences encoding for three fluorescent proteins, mCherry, YPet, and Turquoise fluorescent protein (TFP), respectively [24,25]. Single cell clones were picked, and selected for further analyses based on their basal and inducible Nrf2, HIF, and NF-κB activity. Five different HCT[(pTRAFNrf2/HIF/NFkB)] clones were studied in parallel. To monitor transcription factor activities of 2D cultures, cells were seeded at a density of 30,000 cells per well of a black 96-well plate (Thermo Fisher, 165305). The day after, cells were exposed to 2 and 10 ng/ml tumor necrosis factor alpha in 3D and 2D cultures respectively (TNFα, Sigma Aldrich), 1 or 2 μM auranofin for qPCR and 2D/3D cultures respectively (AUR, Enzo Life science), 250 μM dimethyloxalylglycine (DMOG, Sigma Aldrich), 10 μM rosiglitazone (ROSI, Sigma Aldrich), or 10 mM lithium chloride (LiCl, Sigma Aldrich) for 20 h. Nuclei were stained with 40 ng/ml Hoechst (Life technologies). For 3D cultures, the HCT[(pTRAFNrf2/HIF/NFkB)] clones were seeded as described above and 3 days after seeding, spheroids were treated (Fig. S1B). Transcription factor activities were monitored over time in living spheroids using the Operetta HTS system, an automatized fluorescent, confocal microscope (Perkin Elmer). In confocal mode, we screened 10 confocal layers. The Columbus software was used to quantify fluorescence intensities and Image J to measure spheroid size.

2.4. Statistics

Data are shown as mean + SD. All treatments were performed at least in duplicates per plate. Accordingly, the mean was calculated out of the four individual clones in case of the pTRAF fluorescent experiments. For qPCR (measured in triplicate) and Western Blot analyses, three independent experiments were performed with one selected clone and averaged thereafter. Statistical significance was calculated by GraphPad Prism version 6 using oneway analysis of variance (ANOVA) with Tukey's multiple comparisons test or unpaired Student's *t*-test as indicated in figure legends. A p-value < 0.05 was considered as statistically significant.

3. Results and discussion

3.1. Spheroid formation promotes cancer stem cell characteristics

We first characterized the cellular phenotypes of our HCT(pTRAF[Nrf2/HIF/NFkB])-derived clones during spheroid formation (Fig. 1A). After 24 h of culturing under 3D conditions, the HCT(pTRAF[Nrf2/HIF/NFkB]) cells increased their expression of well-established stemness markers such as NANOG, AXIN2, LGR5, CD44, and CD133 (Fig. 1A). CD44 and CD133 expression indicate subpopulations of cells capable to establish tumors upon implantation in immune deficient hosts [26,27]. This property was also shown for LGR5-expressing cells, initially identified as intestinal stem cells [28]. Both LGR5, the co-receptor for the WNT ligand R-spondin, and AXIN2, are target genes of β-catenin/TCF. Especially in colon, β-catenin activity is also considered as a suitable CSC marker [29]. AXIN2 showed an almost 30-fold increase in expression during the first day of spheroid formation, clearly indicating that Wnt signaling was further activated. NANOG was chosen to extend the signature to contain a marker for
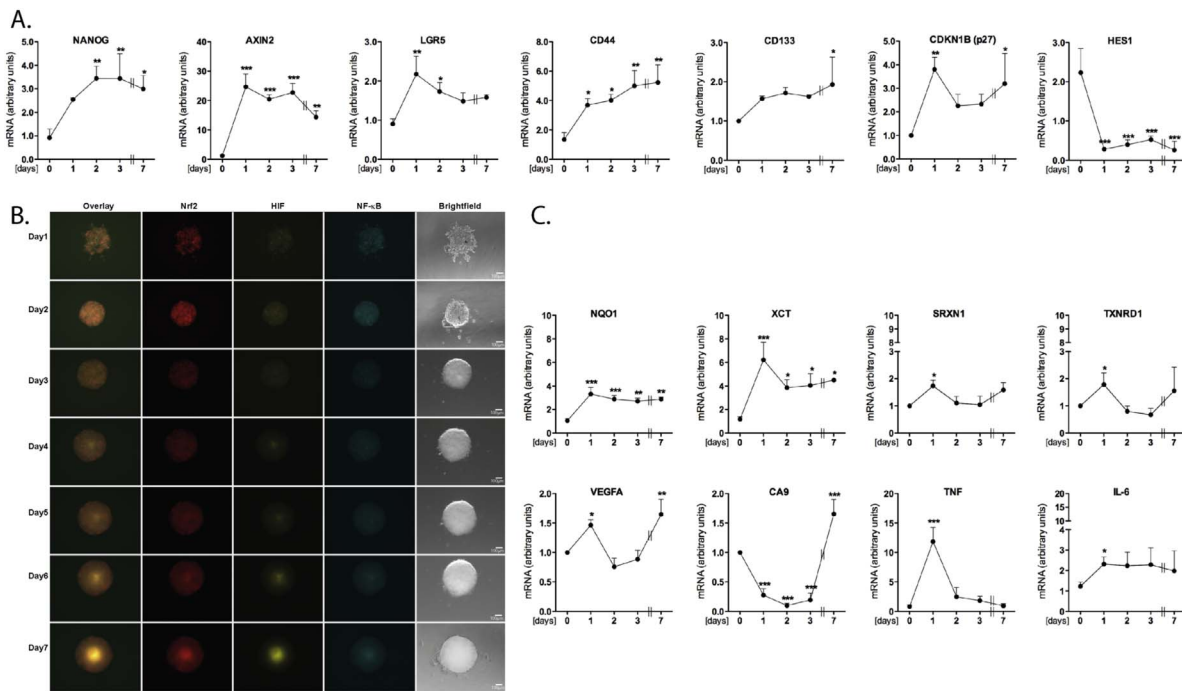
Fig. 1. Stem cell markers expressed in synergy to Nrf2, HIF and NF-κB activation during spheroid formation. (A) The mRNA expression of stem cell markers in spheroids was measured 1, 2, 3 and 7 days after seeding. The mRNA levels of NANOG, AXIN2, LGR5, CD44, CD133, CDKN1B (p27), and HES1 were analyzed in triplicate by qPCR and normalized to the reference gene RPL13A. (B) Fluorescent pictures to monitor the activity of Nrf2, HIF and NF-κB during spheroid formation using HCT(pTRAF[Nrf2/HIF/NFkB]) clones. Red color indicates Nrf2 activity, yellow HIF, and cyan indicates NF-κB activity. (C) After 1, 2, 3 and 7 days of seeding cells as spheroids, mRNA expression of Nrf2 (NQO1, XCT, SRXN1, and TXNRD1), HIF (VEGFA, CA9) and NF-κB downstream target genes (TNF, IL-6) was analyzed in triplicate by qPCR and normalized to the reference gene RPL13A. Data are shown as mean + SD (n =3). Significant differences were calculated in comparison to adherent cells (day 0) using one-way ANOVA with Tukey's post-test: *$p < 0.05$; **$p < 0.01$; ***$p < 0.001$. Scale bars in the brightfield images represent 100 μm.

undifferentiated cells first established for embryonic stem cells [2]. These two markers remained increased in the developing spheroids for 7 days upon seeding and this up-regulation was accompanied by enhanced expression of the cell cycle inhibitor p27 (CDKN1B; cyclin-dependent kinase inhibitor 1B). Indeed, many cyclin-dependent kinase inhibitors are expressed in quiescent stem cells and promote cell cycle arrest [30]. Furthermore, the NOTCH target gene HES1 was strongly down-regulated (Fig. 1A) upon spheroid formation. In the intestine, NOTCH signaling is of importance to regulate the balance between rapidly and slowly cycling stem cell populations [31]. Especially HES1 is essential for the enterocyte-secretory fate switch thus promoting differentiation into enterocytes [32]. Down-regulation of HES1 during spheroid formation should thus indicate their switch to a phenotype with reduced capacity to differentiate. These expression patterns strongly suggest that an increased proportion of quiescent CSCs developed over time in our spheroid model.

3.2. During early spheroid formation, redox-regulated transcription factors are activated in parallel with the appearance of stem cell markers

The use of HCT(pTRAF[Nrf2/HIF/NFkB]) clones enabled us to follow Nrf2, HIF and NF-κB activities using fluorescence, thereby allowing for spatiotemporal determinations in developing spheroids. In parallel with the increases in stem cell and quiescence marker expression 1–2 days after seeding (Fig. 1A), Nrf2, HIF, and NF-κB activities were induced throughout the whole spheroids (Fig. 1B, see Fig. S1C for quantification). At an early stage of spheroid formation, apoptosis/anoikis induction was indeed indicated by down-regulation of BIRC3 (cIAP2) a member of the inhibitor of apoptosis family (Fig. S1D). An increase in H_2O_2 production was discussed as a mechanism to overcome anoikis [33], which would be compatible with the initial activation of Nrf2, HIF and NF-κB. Between days 3–5, the activities of the

three transcription factors were subsequently reduced. The utilized fluorescence reporter proteins have similar half-lives thus enabling comparisons in dynamics of the three signals over time [24]. To validate these pTRAF-derived results we also analyzed expression patterns of Nrf2, HIF and NF-κB target genes. The four Nrf2 targets NQO1, XCT, SRXN1, and TXNRD1 showed corresponding increases with highest expression levels on day 1 after seeding (Fig. 1C). NQO1 and XCT, a cystine-glutamate exchange transporter that elevates intracellular cysteine levels and promotes synthesis of GSH (33) displayed the highest fold change in comparison to 2D cultures, i.e. at seeding (day 0). The antioxidant enzymes SRXN1 and TXNRD1 as well as XCT, reduce oxidative stress and thus subsequently counter regulate Nrf2 activity. Interestingly, a variant isoform of the stem cell marker CD44 (CD44v) was found to stabilize xCT and thus to improve its function [34]. Accordingly, CD44^{low} cells are characterized by oxidative stress in comparison to CD44^{high} cells. It has also been discussed that Nrf2 is essential to maintain the quiescence state of hematopoietic stem cells [35] and Drosophila intestinal stem cells by keeping them in a reduced redox state [19]. The HIF target VEGFA was also significantly up-regulated on day 1, while carbonic anhydrase IX (CA9) was down-regulated during this early phase of spheroid formation (Fig. 1C). The NF-κB target genes TNF and IL-6 were also significantly up-regulated on day 1 and subsequently reduced (Fig. 1C). Thus, the pTRAF signals (Fig. 1B) agreed with the qPCR results (Fig. 1C), revealing early activation of the three redox-regulated transcription factors Nrf2, HIF and NF-κB upon initiation of spheroid formation, taking place at the same time as enhanced expression of stemness markers (Fig. 1A).

3.3. HIF and Nrf2 are specifically activated in the core of larger spheroids

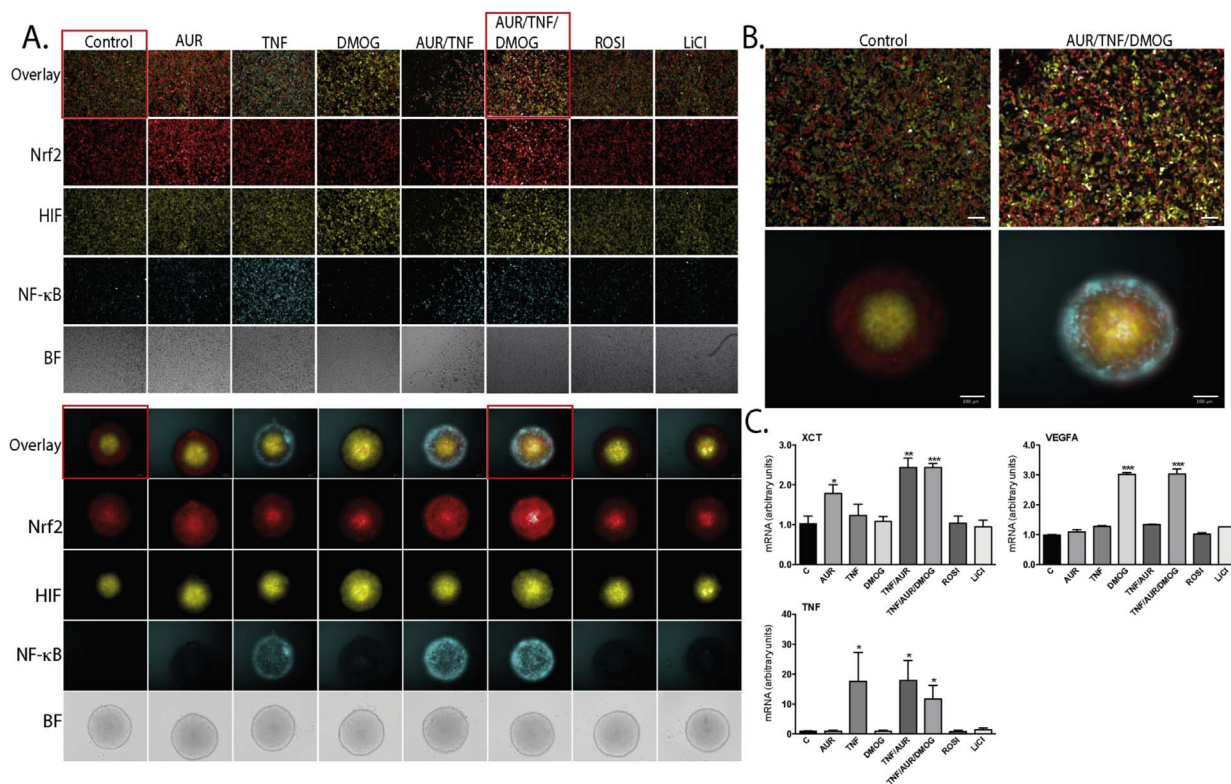At days 6–7 after seeding, HIF and, interestingly, also Nrf2, were

Fig. 2. Stimulation of Nrf2, HIF, and NF-κB in 2D and 3D cultured cells. HCT(pTRAF$^{Nrf2/HIF/NFkB}$) reporter cells grown either as 2D adherent cultures (A) or as 3D spheroids (B) were exposed for 20 h to the Nrf2 inducer AUR (2 μM), the NF-κB inducer TNFα (2 and 10 ng/ml for 3D and 2D cultures, respectively), the HIF inducer DMOG (250 μM), the combination of AUR/TNF and AUR/TNF/DMOG (the same concentrations as for single treatments), the PPAR agonist ROSI (10 μM), or the Wnt inducer LiCl (10 mM). The 2D cultured cells were stimulated 1 day after seeding and the 3D spheroids 3 days after seeding and brightfield (BF) as well as fluorescent pictures were taken. The red color indicates Nrf2 activity, yellow HIF, and cyan indicates NF-κB activity. The white scale bar in the right corner of the enlarged fluorescent pictures represents 100 μm. (C) mRNA expression of HCT(pTRAF$^{Nrf2/HIF/NFkB}$) reporter cells grown as spheroids. Target genes of Nrf2 (XCT), HIF (VEGFA), and NF-κB (TNF) were analyzed in triplicate by qPCR and normalized to RPL13A and HPRT. Data are shown as mean + SD (n =3). Significant differences were calculated in comparison to untreated control cells using unpaired *t*-test: *p < 0.05; **p < 0.01; ***p < 0.001.

markedly activated in the cores of the spheroids (Fig. 1B). Activation of HIF was earlier shown to be trigged by hypoxia in the inner parts of larger spheroids [22]. In good correlation, the HIF targets VEGFA and CA9 were also further up-regulated on day 7 after seeding (Fig. 1C). Concomitant activation of Nrf2 in cores of growing spheroids, as found here, has however not been known. In line with this observation, also the expression of Nrf2 targets (Fig. 1C) remained up-regulated over time (NQO1 and XCT), or even showed a bi-phasic response (SRXN1), suggesting that the expression of these genes at the later time points predominantly occurred in the cores of the mature spheroids (Fig. 1B). Nrf2 has been described to interact with both Wnt and Notch signaling [36,37]. Our determination of Nrf2 activation patterns during the development of spheroids together with previous results suggests that Nrf2 is a key determinant for stemness. The finding that Nrf2 and HIF both become activated in the core of mature spheroids may prove important. It should be noted that NF-κB was not activated in this latter phase, in contrast to that seen during day 1, illustrating specific mechanisms rather than an overall activation of redox-sensitive transcription factors. For the survival of a cancer cell, balancing between signaling and damaging effects of H_2O_2 appears to be a crucial factor [38]. We have thus here helped to decipher the outcome of such redox signaling in terms of the localization and dynamics of Nrf2, HIF and NF-κB activation during the development of multicellular spheroids. Next we aimed to investigate the activity of Nrf2, HIF and NF-κB after different treatments in both 3D spheroid and 2D adherent cultures.

3.4. Nrf2, HIF and NF-κB become highly coordinated under 3D culture conditions in strong contrast to their stochastic activation patterns in 2D cultures

Using the pTRAF reporter system, we previously showed that HEK293, A431 and HCT116 cells display heterogeneous stochastic activation patterns for Nrf2, HIF and NF-κB when grown as adherent cells in 2D cultures [24]. Comparing 2D and 3D cultures of the very same HCT(pTRAF$^{Nrf2/HIF/NFkB}$) clone (Fig. 2A and B), the same heterogeneity was found here in 2D culture (Fig. 2A and B, controls) while spheroid formation induced a highly coordinated activation pattern. After three days of development Nrf2 activity could be detected throughout the spheroids, HIF activity was predominately localized within the core while NF-κB activity was almost undetectable under untreated conditions (Fig. 2B, controls). Using pTRAF, we showed previously that the endogenous activity of Nrf2, HIF and NF-κB is higher in HCT116 in comparison to HEK293 cells [24]. However, even though basal activities of the three transcription factors were relatively high, they could be further increased by exposing HCT cells to known inducers of any of the three transcription factors (Fig. S1B for experimental setup; Fig. S2A and B for consistency in results with individual clones). Treatment with AUR as a well-established Nrf2 inducer [39] resulted in activation of Nrf2 at 24 h after treatment in both 2D (Fig. 2A and S2C upper panel) and spheroid (Fig. 2A and S2C lower panel) cultures. In spheroid cultures this Nrf2 activation occurred throughout the whole cell mass, with HIF and NF-κB being essentially unaffected, resulting in overlay pictures with strong fluorescence of both yellow and red in the core of the spheroids (HIF and Nrf2 activities in the core) with an outer red ring (Nrf2 activation also in the outer regions). In contrast, the effects of TNFα treatment that
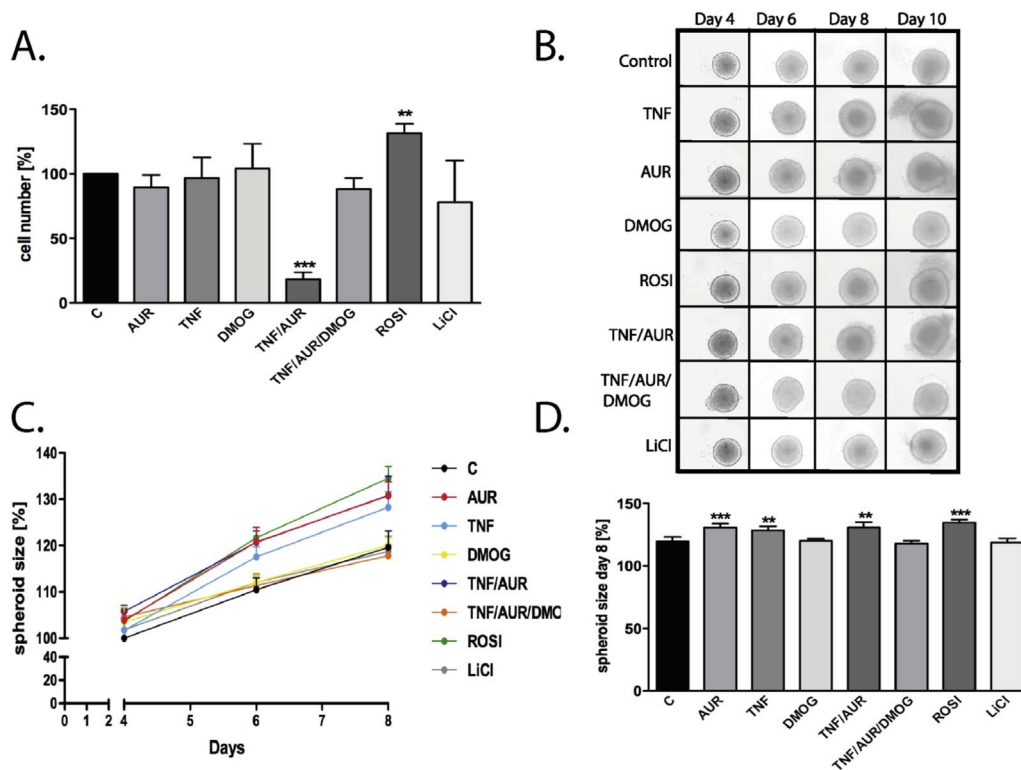
Fig. 3. Growth and viability of 2D and 3D cultures in response to drug treatments. (A) Cell number quantified by Hoechst staining of HCT(pTRAF$^{Nrf2/HIF1/NFkB}$) reporter cells grown adherently and exposed to indicated drugs for 20 h. The data is shown in percent relative to the control (on average 18,000 cells per well). (B) Phase contrast pictures of HCT(pTRAF$^{Nrf2/HIF/NFkB}$) spheroids after stimulation with TNFα (2 ng/ml), AUR (2 μM), DMOG (250 μM), ROSI (10 μM), LiCl (10 mM), TNF/DMOG, and TNF/AUR/DMOG on day 4 (24 h after treatment), 6 (3 d after treatment), 8 (5 days after treatment), and 10 (7 days after treatment) after seeding (See experimental setup Fig. S1B). Pictures of all four individual clones are shown in Fig. S2. (C) Growth rate of spheroids over time. The size of individual spheroids was analyzed by ImageJ and calculated for each time point as percentage of the size before treatment (day 3). (D) The bar diagram shows spheroid size on day 8. Data are shown as mean + SD (n =4). Significant differences were calculated in comparison to untreated control cells (indicated by C) using unpaired t-test: **p < 0.01; ***p < 0.001.

activated NF-κB was detectable in the whole spheroid but more strongly induction at the surface of the spheroids, resulting in an intense outer rim of blue fluorescence (Fig. 2A lower panel). Upon treatment with DMOG, a competitive inhibitor of PHD, an exaggerated activation of HIF was detected as increased yellow fluorescence, observed also under these non-hypoxic conditions in 2D cultures (Fig. 2A upper panel) and throughout whole spheroids but extra strong in the spheroid cores (Fig. 2A lower panel and Fig. S3A for confocal pictures). Interestingly, combining TNFα and AUR treatment was very toxic in adherent 2D culture (Fig. 2A), while the addition of DMOG to TNFα and AUR rescued the cells from toxicity. However, acute cytotoxic effects of the combined TNF/AUR treatment were absent in spheroids, indicating a higher inherent resistance to challenge (Fig. 2A). Combining TNF, AUR and DMOG clearly resulted in a stronger Nrf2 response in comparison to single AUR treatment in 2D cultures, together with further enhanced HIF responses (Fig. 2A and S2C). Finally, treating cells with the Wnt inducer LiCl or the PPAR ligand rosiglitazone (ROSI) did not affect any of the three transcription factors, thus confirming specificity in the readouts (Fig. 2A). To further validate the three transcription factor responses in the spheroids, as illustrated by the pTRAF-derived fluorescent signals, expression of known target genes for Nrf2, HIF, and NF-κB were also analyzed by qPCR using lysates of whole similarly treated spheroids, the readout of which confirmed the anticipated activation patterns (Fig. 2C).

3.5. Growth-promoting effects of TNFα and AUR on 3D spheroids

As stated above, treatment of 2D adherent cells with a combination of TNF/AUR was cytotoxic, with substantially reduced cell numbers, while, interestingly, addition of DMOG to the same concentrations of TNF/AUR abolished this effect. Thus, HIF activation in the 2D cultured

cells seems to protect them from the toxic effects of combining TNF with AUR. Treatment with the PPAR ligand ROSI, known to induce proliferation, significantly increased the cell numbers in 2D cultures, as expected (Fig. 3A). In contrast to the effects observed in 2D cultures, spheroid size increased after single AUR or TNF, and the combination AUR/TNF as well as ROSI treatments (Fig. 3B–D). At later time points cells detached from the spheroids that hence lost their smooth appearances under these conditions (day 8 and 10; Fig. 3B and Fig. S3B). Again, the effect of the combined TNF/AUR treatment was prevented by simultaneous addition of DMOG. The size and growth of DMOG- and LiCl-treated spheroids were thereby comparable to untreated controls irrespective of any additional treatment (Fig. 3B–D).

3.6. AUR induces proliferating differentiated spheroids while DMOG triggers a highly resistant quiescent phenotype

To further characterize spheroid properties after treatment, expression levels of markers were evaluated (Fig. 4). In such experiment, short-term (4 h) changes should mainly result from altered transcription levels, while long-term (3 d) effects can also reflect shifts in cell populations within the spheroids. Out of the three stem cell markers NANOG, AXIN2, and CD44, only AXIN2 was induced after 4 h of LiCl treatment (Fig. 4A), above its already high expression in spheroids as compared to 2D cultures (Fig. 1A). However, 3 days after LiCl treatment the expression of all stem cell markers was induced, indicative of an increased proportion of CSCs (Fig. 4B). Besides that, only DMOG increased expression of CD44 after 3 days of treatment, as well as of the quiescence marker p27 4 h after treatment (Fig. 4A). Furthermore, the proliferation-associated PCNA protein and the differentiation marker mucin2 (MUC2) displayed low expression 3
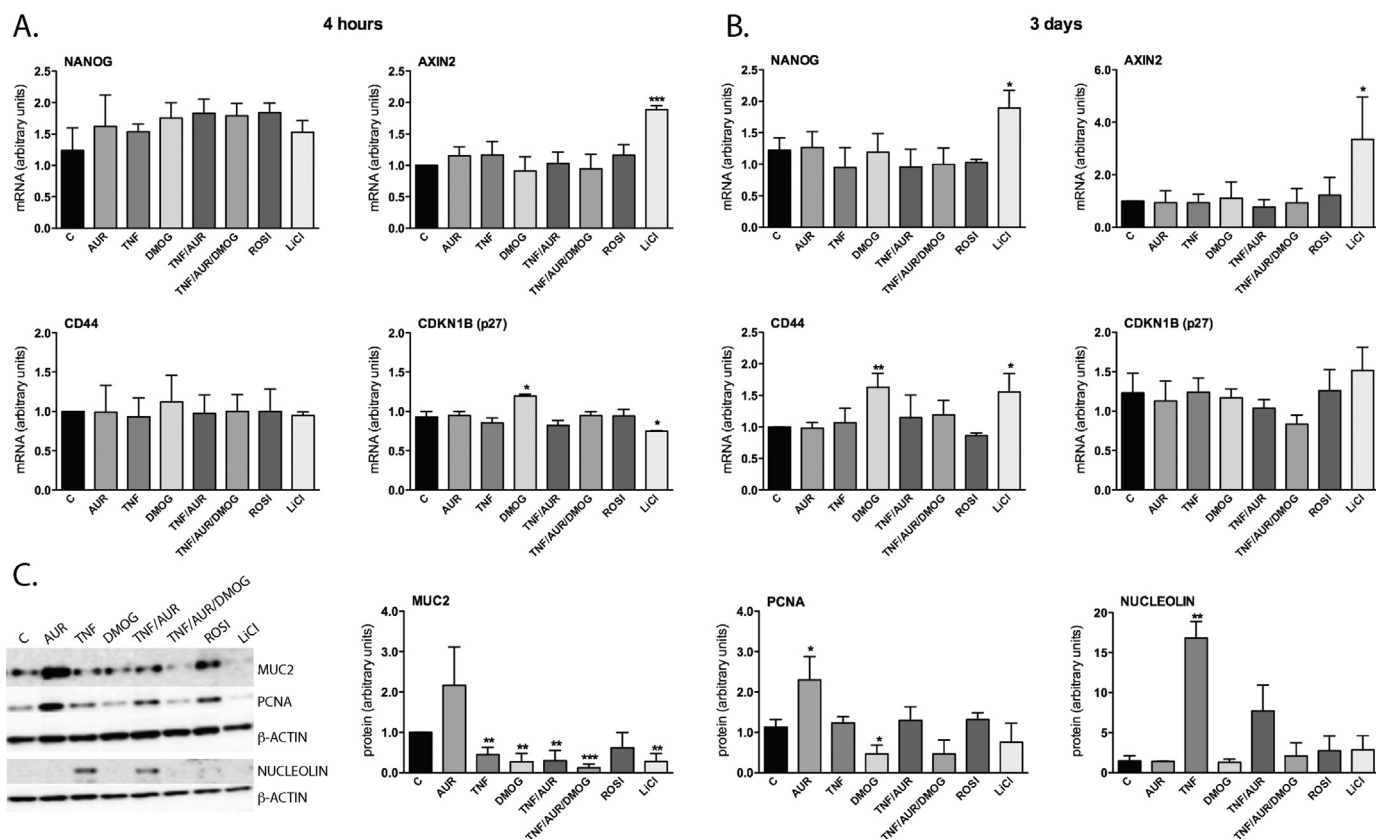
Fig. 4. Changes of stem cell and differentiation markers after drug treatments. mRNA expression of HCT(pTRAF^Nrf2/HIF/NFkB) reporter cells grown as spheroids and exposed to TNFα (2 ng/ml), AUR (1 μM), DMOG (250 μM), ROSI (10 μM), LiCl, (10 mM), TNF/DMOG, and TNF/AUR/DMOG for 4 h (A) or 3 days (B). NANOG, AXIN2, CD44, and CDKN1B (p27) were analyzed in triplicate by qPCR and normalized to RPL13A and HPRT. (C) Protein expression of PCNA, MUC2, and Nucleolin was analyzed by Western Blot 3 days after treatment (day 6 after seeding) and normalized to β-Actin. Data are shown as mean + SD (n =3; n =2 for Nucleolin Western Blot). Significant differences were calculated in comparison to untreated control cells (indicated by C) using unpaired *t*-test: *p < 0.05; **p < 0.01; ***p < 0.001.

days after DMOG treatment (Fig. 4C), which also suggests enrichment for CSC-like quiescent cells that should explain the small size (Fig. 3D) and resistant (Fig. 3B) phenotype. In contrast, PCNA and MUC2 levels were high in AUR-treated spheroids (Fig. 4C) compatible with the notion that their increased size was due to increased cell proliferation. Also the proliferation marker nucleolin (NCL) was induced upon treatment with TNF or TNF/AUR, but unaffected by all other treatments including TNF/AUR with the addition of DMOG (Fig. 4C), in close agreement with the overall quiescent and resistance phenotype of spheroids treated with all three agents (Fig. 3). Thus, even though Nrf2, HIF, and NF-κB were activated during spheroid formation (Fig. 1), only stimulation with DMOG appeared to increase the proportion of CSCs. Inhibitory effects of hypoxia and DMOG treatment on colon CSC differentiation have indeed been described previously [40]. Herein, we found that DMOG was dominant over the phenotypes triggered by AUR or TNF. AUR stimulation, instead, clearly directed cells towards a differentiated proliferating phenotype, which was not observed in the combined TNF/AUR treatment (Fig. 4). AUR is in clinical trials as an anti-cancer drug, and is known to have pro-oxidative effects at high concentrations [41]. Shifting CSCs to a more differentiated phenotype could indeed be beneficial for therapy, as the latter are typically more sensitive to anticancer treatments. In this context, it is worth noting that many standard forms of cancer therapy, such as irradiation and chemotherapy, involve the induction of oxidative stress [5,42,43]. Also TNFα resulted in an increase in spheroid size, but in contrast to AUR and ROSI no significant induction of MUC2 and PCNA were shown. In contrast, another proliferation marker, NCL was upregulated, suggesting that AUR and TNFα promote cellular proliferation via different mechanisms.

4. Conclusion

In the present report, we have mapped the spatiotemporal dynamics in activation patterns of Nrf2, HIF, and NF-κB during spheroid formation, established from individual clones of HCT116 cells. For the first time we could show evident coordination of redox-sensitive pathways in 3D spheroids in relation to overall phenotype. We found that mature spheroids activate both HIF and Nrf2 in their cores, and that an increase in the proportion of resistant and quiescent CSCs could be provoked by DMOG treatment in parallel with a further pronounced HIF activation. This effect was unaltered by simultaneous treatment with TNF or AUR, which otherwise resulted in a proliferative phenotype in established spheroids. These observations should be of major importance for the understanding of tumor biology, and the model system established here should be of significant use for future studies.

Appendix A. Supplementary material

Supplementary data associated with this article can be found in the online version at doi:10.1016/j.redox.2017.03.013.

References

[1] C.A. O'Brien, et al., A human colon cancer cell capable of initiating tumour growth in immunodeficient mice, Nature 445 (7123) (2007) 106–110.

[2] I. Ben-Porath, et al., An embryonic stem cell-like gene expression signature in poorly differentiated aggressive human tumors, Nat. Genet. 40 (5) (2008) 499–507.

[3] T.P. Szatrowski, C.F. Nathan, Production of large amounts of hydrogen-peroxide by human tumor-cells, Cancer Res. 51 (3) (1991) 794–798.

[4] D. Trachootham, et al., Selective killing of oncogenically transformed cells through a ROS-mediated mechanism by beta-phenylethyl isothiocyanate, Cancer Cell 10 (3) (2006) 241–252.

[5] D. Trachootham, J. Alexandre, P. Huang, Targeting cancer cells by ROS-mediated mechanisms: a radical therapeutic approach?, Nat. Rev. Drug Discov. 8 (7) (2009) 579–591.

[6] R. Brigelius-Flohe, L. Flohe, Basic principles and emerging concepts in the redox control of transcription factors, Antioxid. Redox Signal 15 (8) (2011) 2335–2381.

[7] C. Ufer, et al., Redox control in mammalian embryo development, Antioxid. Redox Signal 13 (6) (2010) 833–875.

[8] S. Ding, et al., Redox regulation in cancer stem cells, Oxid. Med. Cell Longev. 2015 (2015) 750798.

[9] S. Schwitalla, et al., Intestinal tumorigenesis initiated by dedifferentiation and acquisition of stem-cell-like properties, Cell 152 (1–2) (2013) 25–38.

[10] S.I. Goktuna, et al., The prosurvival IKK-related kinase IKK epsilon integrates LPS and IL17A signaling cascades to promote Wnt-dependent tumor development in the intestine, Cancer Res. 76 (9) (2016) 2587–2599.

[11] K.B. Myant, et al., ROS production and NF-kappa B activation triggered by RAC1 facilitate WNT-driven intestinal stem cell proliferation and colorectal cancer initiation, Cell Stem Cell 12 (6) (2013) 761–773.

[12] G.L. Wang, G.L. Semenza, Purification and characterization of Hypoxia-Inducible Factor-1, J. Biol. Chem. 270 (3) (1995) 1230–1237.

[13] K.M. Govaert, et al., Hypoxia after liver surgery imposes an aggressive cancer stem cell phenotype on residual tumor cells, Ann. Surg. 259 (4) (2014) 750–759.

[14] E.S. Arner, Focus on mammalian thioredoxin reductases–important selenoproteins with versatile functions, Biochim. Biophys. Acta 1790 (6) (2009) 495–526.

[15] J.M. Hansen, W.H. Watson, D.P. Jones, Compartmentation of Nrf-2 redox control: regulation of cytoplasmic activation by glutathione and DNA binding by thioredoxin-1, Toxicol. Sci. 82 (1) (2004) 308–317.

[16] H. Satoh, et al., NRF2 intensifies host defense systems to prevent lung carcinogenesis, but after tumor initiation accelerates malignant cell growth, Cancer Res. 76 (10) (2016) 3088–3096.

[17] I. Ganan-Gomez, et al., Oncogenic functions of the transcription factor Nrf2, Free Radic. Biol. Med. 65 (2013) 750–764.

[18] Y. Mitsuishi, H. Motohashi, M. Yamamoto, The Keap1-Nrf2 system in cancers: stress response and anabolic metabolism, Front Oncol. 2 (2012) 200.

[19] C.E. Hochmuth, et al., Redox regulation by Keap1 and Nrf2 controls intestinal stem cell proliferation in Drosophila, Cell Stem Cell 8 (2) (2011) 188–199.

[20] K.L. Chen, et al., Highly enriched CD133(+)CD44(+) stem-like cells with CD133(+)CD44(high) metastatic subset in HCT116 colon cancer cells, Clin. Exp. Metastas-. 28 (8) (2011) 751–763.

[21] T.M. Yeung, et al., Cancer stem cells from colorectal cancer-derived cell lines, Proc. Natl. Acad. Sci. USA 107 (8) (2010) 3722–3727.

[22] F. Hirschhaeuser, et al., Multicellular tumor spheroids: an underestimated tool is catching up again, J. Biotechnol. 148 (1) (2010) 3–15.

[23] B.L. Emmink, et al., Differentiated human colorectal cancer cells protect tumor-initiating cells from Irinotecan, Gastroenterology 141 (1) (2011) 269–278.

[24] K. Johansson, et al., Cross talk in HEK293 cells between Nrf2, HIF, and NF-kappaB activities upon challenges with Redox therapeutics characterized with single-cell resolution, Antioxid. Redox Signal 26 (6) (2017) 229–246.

[25] J. Goedhart, et al., Structure-guided evolution of cyan fluorescent proteins towards a quantum yield of 93%, Nat. Commun. 3 (2012) 751.

[26] P. Dalerba, et al., Phenotypic characterization of human colorectal cancer stem cells, Proc. Natl. Acad. Sci. USA 104 (24) (2007) 10158–10163.

[27] L. Vermeulen, et al., Single-cell cloning of colon cancer stem cells reveals a multi-lineage differentiation capacity, Proc. Natl. Acad. Sci. USA 105 (36) (2008) 13427–13432.

[28] N. Barker, et al., Identification of stem cells in small intestine and colon by marker gene Lgr5, Nature 449 (7165) (2007) 1003–1007.

[29] J.P. Medema, Cancer stem cells: the challenges ahead, Nat. Cell Biol. 15 (4) (2013) 338–344.

[30] T.H. Cheung, T.A. Rando, Molecular regulation of stem cell quiescence, Nat. Rev. Mol. Cell Biol. 14 (6) (2013) 329–340.

[31] T. Srinivasan, et al., Notch signalling regulates asymmetric division and inter-conversion between lgr5 and bmi1 expressing intestinal stem cells, Sci. Rep. 6 (2016).

[32] T. Sato, H. Clevers, Growing self-organizing mini-guts from a single intestinal stem cell: mechanism and applications, Science 340 (6137) (2013) 1190–1194.

[33] P. Paoli, E. Giannoni, P. Chiarugi, Anoikis molecular pathways and its role in cancer progression, Biochim. Biophys. Acta-MolecularActa Cell-Mol. Cell Res. 1833 (12) (2013) 3481–3498.

[34] T. Ishimoto, et al., CD44 variant regulates redox status in cancer cells by stabilizing the xCT subunit of system xc(-) and thereby promotes tumor growth, Cancer Cell 19 (3) (2011) 387–400.

[35] X.K. Shi, et al., Reactive oxygen species in cancer stem cells, Antioxid. Redox Signal. 16 (11) (2012) 1215–1228.

[36] N. Wakabayashi, D.V. Chartoumpekis, T.W. Kensler, Crosstalk between Nrf2 and Notch signaling, Free Radic. Biol. Med 88 (Pt B) (2015) 158–167.

[37] R. Brigelius-Flohe, A.P. Kipp, Selenium in the redox regulation of the Nrf2 and the Wnt pathway, Methods Enzym. 527 (2013) 65–86.

[38] T.S. Wu, et al., X-ray absorption study of ceria nanorods promoting the dispro-portionation of hydrogen peroxide, Chem. Commun. 52 (28) (2016) 5003–5006.

[39] K. Kataoka, H. Handa, M. Nishizawa, Induction of cellular antioxidative stress genes through heterodimeric transcription factor Nrf2/small Maf by antirheumatic gold(I) compounds, J. Biol. Chem. 276 (36) (2001) 34074–34081.

[40] N. Ashley, T.M. Yeung, W.F. Bodmer, Stem cell differentiation and lumen formation in colorectal cancer cell lines and primary tumors, Cancer Res. 73 (18) (2013) 5798–5809.

[41] X. Chen, et al., Novel use of old drug: anti-rheumatic agent auranofin overcomes imatinib-resistance of chronic myeloid leukemia cells, Cancer Cell Micro. 1 (6) (2014).

[42] S. Powell, T.J. Mcmillan, DNA damage and repair following treatment with ionizing-radiation, Radiother. Oncol. 19 (2) (1990) 95–108.

[43] C.E. Myers, et al., Adriamycin: the role of lipid peroxidation in cardiac toxicity and tumor response, Science 197 (4299) (1977) 165–167.